Paper AAS 06-102

IN-FLIGHT ESTIMATIONS OF CASSINI SPACECRAFT INERTIA TENSOR AND THRUSTER MAGNITUDE

Antonette Feldman and Dr. Allan Y. Lee
Jet Propulsion Laboratory, California Institute of Technology

16th AAS/AIAA Space Flight Mechanics Conference

Tampa, Florida **January 22-26, 2006**

AAS Publications Office, P.O. Box 28130, San Diego, CA 92198

Launched on October 15th, 1997 and arriving at Saturn on June 30th, 2004, Cassini is the largest and most sophisticated interplanetary spacecraft ever built. Meeting the challenging requirements of the Cassini Attitude and Articulation Control Subsystem requires knowledge of the spacecraft's inertia matrix as well as thrusters' magnitude. This paper describes two methods used by the Cassini Attitude Control team to determine these key parameters and how flight telemetry was used to estimate them. The method for estimating the spacecraft inertia tensor exploits the conservation of angular momentum during spacecraft slews under reaction wheel control. Spacecraft telemetry provides reaction wheel spin rates and spacecraft's rates; while ground measured inertia properties of the reaction wheels are also used. By collecting data during multi-axis slews, we are able to generate a least-square estimate of the Cassini inertia tensor. A method for estimating the thrust magnitude based on Euler's equation is also discussed. This method uses telemetry data of the reaction wheel spin rates, spacecraft angular velocities, spacecraft quaternion, spacecraft angular momentum, thruster on-times and the previously determined inertia tensor. Results of the applications of these methods on flight data will be given and discussed.

Acronyms

AACS = Attitude and Articulation Control Subsystem
ACC = Accelerometer
ETC = Excessive Thruster Commanding (Error Monitor)
FSDS = Flight Software Development System
FSW = Flight Software
GSW = Ground Software
HGA = High Gain Antenna
LGA = Low Gain Antenna
MOI = Moment of Inertia
mrad = milli-radian (about 0.05729578 degree)
NAC = Narrow Angle Camera
PMD = Propellant Management Device
PRM = Periapse Raise Maneuver
POI = Product of Inertia
RCS = Reaction Control System
rpm = revolutions per minute
RWA = Reaction Wheel Assembly
RWAC = Reaction Wheel Attitude Control System
S/C = Spacecraft

Nomenclature

e_i = Coordinates of Spacecraft's Center of Mass, i = X, Y, and Z (m)
F_i = Thruster magnitude, i = 1,…,8 (N)
H_{RWA} = Angular Momentum Vector of the Reaction Wheels (Nms)
H_{Total} = Total Angular Momentum Vector of the Spacecraft System (Nms)
I_{RWA} = Inertia Tensor of the Reaction Wheels (kg-m^2)
I_{sc} = Inertia Tensor of the Spacecraft (kg-m^2)
N_s = Number of Time Steps (-)
P = Coordinate Transformation Matrix, from Inertial Frame to the Spacecraft Axes (-)
q_i = Euler's Parameters, or Quaternion (i = 1-4)
Q = A time-varying vector defined in Eq. (6) (Nms)
T = Coordinate Transformation Matrix, Reaction Wheel Axes to Spacecraft Axes (-)
ρ = Reaction Wheel Spin Rate Vector (rad/s)
ω = Spacecraft Angular Rate Vector (rad/s)
μrad = Microradian (≈5.729578e-5 degrees)
$\Delta\tau_S(t_i)$ = Incremental On-time of Thruster S (S = Z_1 to Z_4, and Y_1 to Y_4), from t = 0 to t_i (s)

I. Cassini/Huygens Mission to Saturn and Titan

After launch, Cassini began an interplanetary cruise of almost seven years, arriving at Saturn on June 30, 2004. To save propellant, Cassini made several gravity-assist flybys: two at Venus and one each at Earth and Jupiter. Figure 1 shows the interplanetary trajectory design of the Cassini mission.

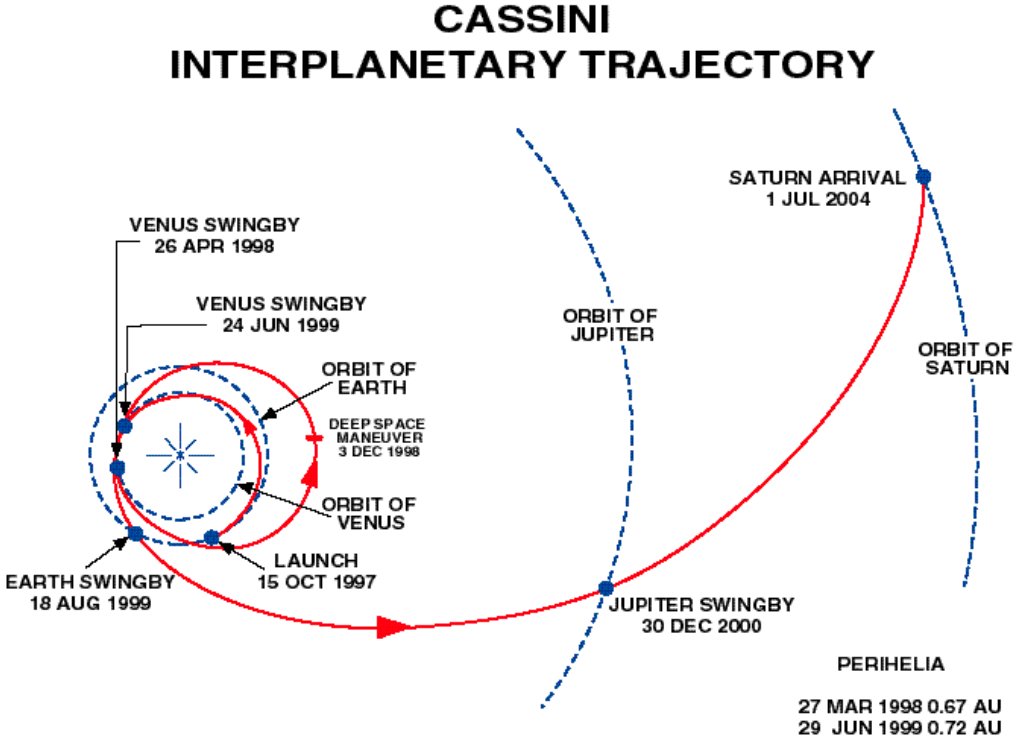

Figure 1. Cassini Interplanetary Trajectory

Unlike Voyagers 1 and 2, which only flew by Saturn, Cassini achieved orbit at Saturn and is scheduled to operate there for a minimum of four years. Major science objectives of the Cassini mission include investigations of the configuration and dynamics of Saturn's magnetosphere, the structure and composition of the rings, the characterization of several of Saturn's icy satellites, and Titan's atmosphere constituent abundance. The radar mapper will perform surface imaging and altimetry during many Titan flybys. Doppler tracking experiments using the Earth and the Cassini spacecraft as separated test masses have also been conducted for gravitational wave searches.[1]

Once at Saturn, Cassini fired one of its two rocket engines for approximately 96 minutes in order to slow down the spacecraft's velocity (by about 626.17 m/s) allowing it to be captured by the gravity field of Saturn. This was the most critical engineering event of the entire mission and was executed faultlessly. After the completion of the Saturn Orbit Insertion (SOI), cameras onboard the spacecraft were used to image Saturn and its rings. Onboard science instruments were also used to study the structure and composition of the rings during both the ascending and descending ring-plane crossings that happened before and after the Saturn Orbit Insertion.[2]

The Huygens Probe, developed by the European Space Agency (ESA), was successfully released on December 24, 2004. At separation, the spin ejection device located on the orbiter imparted on the Probe a spin rate of about 8.1 rpm and a relative velocity of about 0.39 m/s. The Probe was dormant from separation until it reached a Titan-relative altitude of 1270 km, on January 14, 2005. The Probe accelerometers and a radio transmitter were then turned on for measurements during entry. The Probe was first aerodynamically decelerated to Mach 1.5 (approximately 400 m/s) at an altitude of 150-180 km. The heat shield and covers were then jettisoned, and a parachute was deployed. Data was collected over the

descent phase of the Probe mission, about 2 hours and 27 minutes. Data transmission from the Probe, while it was on the surface of Titan, lasted another 1 hour and 12 minutes.

Titan, Saturn's largest moon, is the second largest moon in the Solar System. Only Jupiter's moon Ganymede is larger. At 5150 kilometers in diameter, Titan is larger than either of the planets Mercury or Pluto. Titan orbits Saturn at a distance of 1,222,000 kilometers, taking 15.9 days to complete one revolution. Titan is of great interest to scientists because it is the only known moon in the Solar System with a "major" atmosphere. Titan's atmosphere is 10 times thicker than Earth's. Except for some clouds, Earth's surface is visible from space. But on Titan, a thick haze extending up to 3,000 kilometers above the surface obscures the entire surface from optical observations. Through ongoing observations from Earth as well as data collected by the Pioneer 11 and Voyager 1 and 2 spacecraft, scientists now know that Titan's atmosphere is composed primarily of nitrogen. In fact, over 95% of its atmosphere is composed of nitrogen, while only 5% is composed of methane, cyanide, and other hydrocarbons. The Cassini-Huygens Mission seeks to study Titan via 45 close flybys during its four-year tour of Saturn.

II. Spacecraft Configuration[3]

Measuring about 6.8 m in height with a diameter of 4 meters, the orbiter's total mass at launch was approximately 5574 kg, which includes about 3000 kg of bi-propellant, 1869 kg of Nitrogen Tetroxide, and 1131 kg of mono-methyl hydrazine, 132 kg of high purity hydrazine and 2442 kg of dry mass, which included the 320-kg Huygens Probe and 9 kg of helium mass). Fig. 2 depicts the Cassini spacecraft.

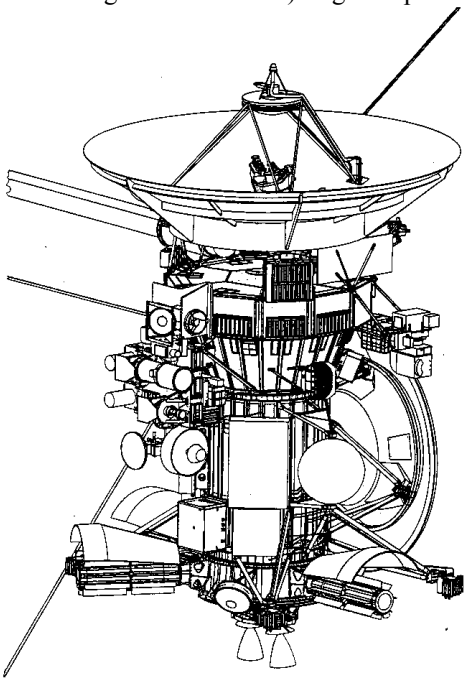

Figure 2. Cassini Cruise Configuration

The base body of the orbiter is a stack consisting of a lower equipment module, a propellant module, an upper equipment module, and a 4-m High Gain Antenna (HGA). Attached to the stack are the Remote Sensing Pallet and the Fields and Particles Pallet with their scientific instruments. Until separation, the Huygens probe was attached to the base body with its axis of symmetry pointed parallel to the negative X-axis of the spacecraft. The orbiter's 12-bay electronics bus is part of the upper equipment module. An 11-m magnetometer boom is mounted to the upper equipment module. At launch, the boom was stowed inside a canister. The magnetometer boom was deployed on August 16, 1999, two days before the Earth swing-by.

The 4-m parabolic HGA and two Low Gain Antennas (LGAs) are the main communication antennas of the spacecraft. An X-band feed, with a maximum engineering data telecommunication rate is 1896 bps, is used for both uplink and downlink communications. An S-band feed was used for communications with the Probe during its descent through the Titan atmosphere. A Ka-band feed is provided for Radio Science. Five Ku-band feeds supply five beams for radar mapping at Titan. For communications, AACS must point

the X-band radio-frequency bore-sight of HGA to Earth. At other times, especially while the spacecraft is in the inner Solar System, AACS must point the HGA axis of symmetry to the Sun so that the antenna will shade most of the spacecraft. During certain hazardous Saturn ring-plane crossings, the HGA axis is pointed parallel to the velocity vector of the orbiter (relative to the ring particles) in order to protect most of spacecraft instruments from the incoming energetic ring particles.

Cassini is a flexible spacecraft containing four structural appendages and three propellant tanks. The four booms are the 11-meter long magnetometer boom and three similar Radio and Plasma Wave Science (RPWS) antennas. The fundamental frequency of the magnetometer boom is 0.7 Hz, and its damping ratio is between 0.2 and 1%. Its second mode frequency is 4 Hz. The RPWS antennas have a fundamental frequency of 0.13 Hz and a damping ratio of 0.2%. Its second mode frequency is 0.86 Hz. The propulsion module houses two cylindrical tanks with hemispherical end domes. These tanks each contain an eight-panel Propellant Management Device (PMD) of the surface tension type. These PMDs are used to control the orientation of the propellant in the low-g environment via surface tension forces. The monopropellant (hydrazine) is kept in a spherical tank that is located off the Z-axis. The tank contains an elastomeric diaphragm for bubble-free expulsion of hydrazine in micro-g condition. The total mass of the hydrazine at launch was about 132 kg.

During early Cruise, Cassini used a set of eight thrusters to control the spacecraft's attitude. Figure 3 (from Reference 5) shows the locations of the four thruster pods that are mounted on a structure attached to the lower equipment module. On each of these pods are mounted two primary thrusters and their backups. Pointing controls about the S/C's X and Y-axis are performed using four Z-facing thrusters. Controls about the Z-axis are performed using four Y-facing thrusters.

Both the Y_2 and Y_4 thrusters must be fired simultaneously, to slew about the positive Z-axis of the spacecraft. Thrusts generated by these firings will almost cancel each other, and the ΔV imparted on the spacecraft will be quite small. Similarly, to slew about the negative Z-axis of the spacecraft both the Y_1 and Y_3 thrusters must be fired simultaneously. Again, the ΔV imparted on the spacecraft will be small. On the other hand, a slew about either the $\pm$X-axis or $\pm$Y-axis will involve firings of the Z-facing thrusters. Since these Z-facing thrusters all point in the same direction, slewing the spacecraft about either the X or Y-axis will generate unwanted ΔV on the spacecraft that must be predicted and incorporated into the designs of the spacecraft trajectory maneuvers.

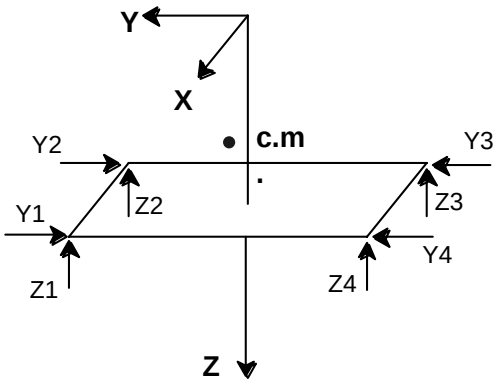

Figure 3. Cassini Thruster Pod Location

During Tour, the spacecraft is slewed using three reaction wheels. To this end, one must assure that both the slew rate and acceleration are consistent with the control authority, power allocation, and the angular momentum capacity of the wheels. The use of reaction wheels has two important merits over the use of thrusters; the absence of unwanted ΔV imparted on the spacecraft and the conservation of hydrazine. A high level of spacecraft pointing stability is needed during imaging operations of high-resolution science instruments such as the Narrow Angle Camera (NAC). Typically, the required level of pointing stability is not achievable with the orbiter controlled by thrusters. Instead, one must employ three Reaction Wheel Assemblies (RWA).

Cassini carries a set of three "strap-down" reaction wheels, mounted on the lower equipment module. They are oriented "equal distance" from the spacecraft's Z-axis. That is, the angle between any of these three RWA's angular momentum vector and the spacecraft's Z-axis is $\cos^{-1}(1/\sqrt{3}) = 54.7356°$. The first use of the reaction wheel control was on March 16, 2000, several months ahead of the Jupiter science campaign that began on October 1, 2000.

A backup reaction wheel is mounted on top of an articulating platform. At Launch, the backup reaction wheel was mounted parallel to reaction wheel 1. On July 11, 2003, the platform was articulated in order to align the backup reaction wheel with reaction wheel 3. Figure 4 depicts the orientations of the four reaction wheels relative to the spacecraft's coordinate frame at Launch.

III. Attitude and Articulation Control System[2]

Perhaps no other spacecraft subsystem must satisfy as many science and mission requirements as the Attitude and Articulation Control Subsystem (AACS). Cassini's AACS estimates and controls the attitude of the three-axis stabilized Cassini spacecraft. It responds to ground-commanded pointing goals for the spacecraft's science instruments and communication antennas with respect to targets of interest. Either thrusters or reaction wheels to slew the spacecraft, the AACS also executes ground-commanded spacecraft velocity changes. To this end, AACS uses either a rocket engine or a set of Z-facing thrusters to effect a velocity change.

The Reaction Wheel Assemblies (RWAs) are used primarily for attitude control when precise and stable pointing of a science instrument (such as NAC) is required during the prime mission phase. RWAs are used to slew the spacecraft from one attitude to another. Once arriving at the targeted attitude, the NAC "stares" at the target for a period of time during which the spacecraft attitude must be stable. As a requirement, the Reaction Wheel Attitude Control System (RWAC)[4] must control the spacecraft with per-axis attitude control errors that are smaller than 40 μrad. Additionally, while under reaction wheel control, the spacecraft pointing stability must be better than those specified in Reference 4. The RWAC design is depicted in Figure 5.

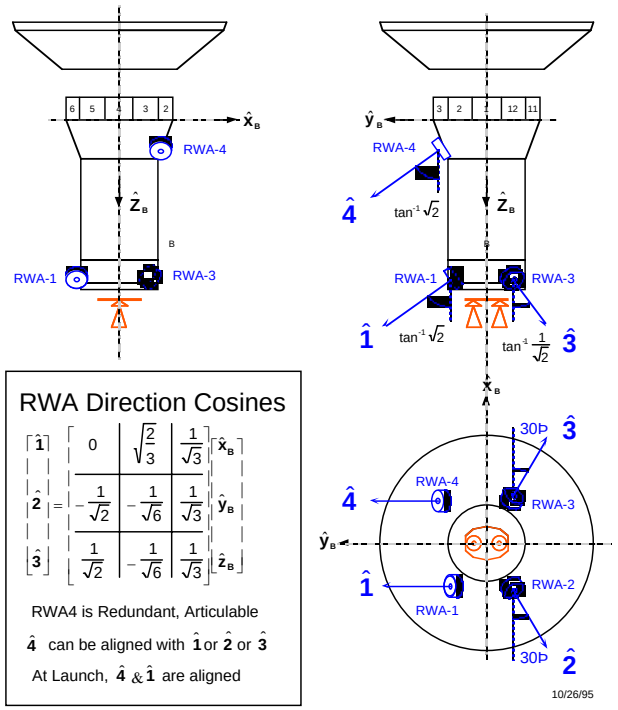

Figure 4. Cassini Reaction Wheel Locations and Orientations

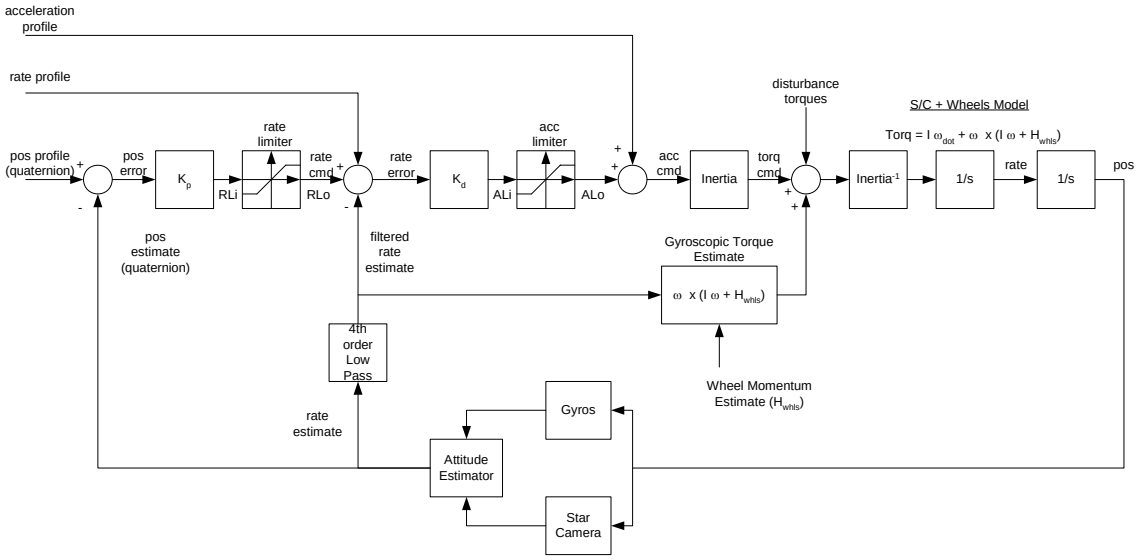

Figure 5. Block Diagram of the Reaction Wheel Attitude Control System (from Reference 4)

Because the spacecraft's principle axes are closely aligned with the spacecraft's mechanical axes, the basic structure of the RWAC is a decoupled, three-axis, Proportional and Derivative (PD) controller. As indicated in Figure 5, the control torque vector is determined using the equation: $I_{SC}d\omega/dt+\omega\times(I_{SC}\omega+H_{RWA})$. Here, I_{SC} is the inertia tensor of the spacecraft, $d\omega/dt$ is the spacecraft's acceleration and ω is the spacecraft rate vector (both vectors are expressed in a body-fixed coordinate frame). The second term in the equation represents the gyroscopic torque vector. The H_{RWA} in the last component of the equation represents the total angular momentum vector of the three prime RWAs expressed in the spacecraft's body-fixed frame. The RWAC is one example in which accurate knowledge of the inertia tensor is needed. Other example will be given in the following paragraph.

An important design feature, depicted in Figure 6, is the addition of the rate and acceleration feed-forward commands. These feed-forward commands generate immediate control action instead of "waiting" for the accumulation of error signals via the feedback loops. As such, the RWAC responses quickly to these profiled slew commands (rather than one without the feed forward signals). The feed-forward command is generated by the Attitude Commander, it derives these signals using commands sent by the spacecraft control team.

IV. In-Flight Estimation of the Spacecraft's Inertia Tensor[5,6]

Several attitude control algorithms on board the Cassini spacecraft use knowledge of the spacecraft's inertia tensor. The inertia tensor is used in the RWAC as described in Section III, it is also used by the Thrust Vector Control (TVC) algorithm.8 The TVC algorithm is used to control the engine gimbal system during a main engine ΔV burn. Additionally, several fault protection error monitor designs such as the "Excessive Thruster Commanding" (ETC) error monitor7 also requires knowledge of the inertia tensor.

The ETC error monitor is used to detect leakage in one of the spacecraft's sixteen thrusters. Implemented as part of the spacecraft flight software, the detection method is based on the fact that the three-axis rotational motion of a spacecraft is governed by Euler's equation. The left-hand-side of Euler's equation contains both the inertia and gyroscopic torque that are estimated by the attitude estimator. The right-hand-side of Euler's equation contains reaction torques from both the thrusters and the reaction wheels. Taking the difference between the left and right hand sides of Euler's equation, and integrating this difference over time, the residual angular momentum vector, attributable to thruster leakage, can be computed. When the absolute value of the residual angular momentum vector grows beyond a pre-selected momentum threshold within pre-selected time duration, a leak is deemed to be present. The identity of the leaking thruster can also be determined using the polarities of the three components of the residual angular momentum vector. Once a thruster leak is detected, remedial actions, such as the swapping of thruster branches can be made to stop the leak.

For uses in the RWAC, ETC, TVC, and other algorithms, it is important to have an accurate estimate of the spacecraft's inertia tensor. Before launch, the inertia tensor was estimated by adding together the moments of inertia of the individual components of the spacecraft. The moments of inertia of individual components were computed with respect to the predicted center of mass of the overall spacecraft before being summed. After launch, the onboard inertia matrix is updated periodically using estimates of how much propellant (both mono and bi-propellant) have been used to date, as well as two discrete events: The deployment of the magnetometer boom and the release of the Huygens Probe. The spacecraft inertia matrix, on March 15, 2000, estimated using the "sum-of-components" method, was:

$$I_{SC} = \begin{bmatrix} 8810.8 & -136.8 & 115.3 \\ -136.8 & 8157.3 & 156.4 \\ 115.3 & 156.4 & 4721.8 \end{bmatrix} \quad \text{kg-m}^2 \tag{1}$$

This estimate of the spacecraft's inertia tensor was not confirmed in-flight until the "conservation of angular momentum" approach that was proposed in References 5 and 6.

The underlying principle of the "conservation of angular momentum" approach is explained as follows, when a spacecraft is slewed using the RWAs, the total angular momentum vector of the spacecraft expressed in an inertial coordinate frame is conserved. This conservation occurs because the addition of angular momentum on the spacecraft due to external torque, such as solar radiation torque, is typically very small over the duration of the slew. On March 15, 2000, the largest per-axis external torque due to all sources was about the spacecraft's X-axis was less than 15 μNm. In the spring of 2005, the total non-gravitational torque has dropped to <2 μNm per-axis. The small size of this non-gravitational torque justifies the "conservation of total angular momentum" assumption made by our approach. Further information on the size of the non-gravitational torque imparted on the spacecraft is given in the Appendix A.

Conservation of angular momentum allows the total angular momentum evaluated just prior to the beginning of the slew to be set equal to the total angular momentum evaluated throughout the slew. This equality gives an equation for each sample time step throughout the slew with only one unknown, I_{SC}, which can then be estimated via a least-squares approach. Note that I_{SC} contains the moments of inertia of the three stationary reaction wheels.

During a spacecraft slew, good estimates of the following quantities are available, either from direct measurement prior to launch or from telemetry data:

(1) Spacecraft angular rates (ω_x, ω_y, and ω_z),
(2) RWA spin rates with respect to its spin axis (ρ_1, ρ_2, and ρ_3),
(3) Spacecraft Euler parameters (q_1, q_2, q_3, and q_4),
(4) Inertia matrix of the three RWAs (I_{RWA}), and
(5) A transformation matrix from the RWA spin axes to the XYZ body coordinate frame (T).

The total angular momentum vector of the spacecraft, expressed in the spacecraft body frame, has two components: $\vec{H}_{Total} = \vec{H}_{SC} + \vec{H}_{RWA}$. The component due to the spacecraft rates is: $\vec{H}_{SC} = I_{SC}\vec{\omega}$ where $\vec{\omega} = [\omega_X, \omega_Y, \omega_Z]^T$. To determine the angular momentum of the RWAs, we first define $\vec{\rho} = [\rho_1, \rho_2, \rho_3]^T$, where ρ_i is the spin rate of the i^{th} RWA about its spin axis. Note that, from March 2000 to July 2003, the prime RWA used were RWA_1, RWA_2, and RWA_3. To find $\vec{H}_{RWA}$, we simply multiply $\vec{\rho}$ first by the inertia matrix for the RWAs, and then multiply by the transformation matrix T. Note that the component of $\vec{H}_{RWA}$ due to spacecraft rates has already been accounted for in $\vec{H}_{SC}$.

$$\vec{H}_{RWA} = TI_{RWA}\vec{\rho} \tag{2}$$

The conservation of angular momentum is only valid in an inertial coordinate system. As such, a transformation matrix, P, defined here from the J_{2000} inertial frame to the body coordinate frame, must be defined. It is computed using the four Euler parameters (q_i, i =1-4). Multiplying the total angular momentum of the spacecraft in body coordinates by the inverse of the transformation matrix P gives the total angular momentum vector in the inertial coordinate frame. The resultant vector, given below, is approximately conserved over a spacecraft slew.

$$\vec{H}_{Total}(t) = P^{-1}(t)I_{SC}\vec{\omega}(t) + P^{-1}(t)TI_{RWA}\vec{\rho}(t) \tag{3}$$

The spacecraft is quiescent just prior to the slew, with all angular rates approximately zero. As such, the initial angular momentum vector is given by:

$$\vec{H}_{Total}(0) = P^{-1}(0) TI_{RWA} \vec{\rho}(0) \tag{4}$$

Invoking the conservation of angular momentum, one gets:

$$P(t)^{-1} I_{SC} \vec{\omega}(t) + P(t)^{-1} TI_{RWA} \vec{\rho}(t) \approx P(0)^{-1} TI_{RWA} \vec{\rho}(0) \tag{5}$$

Now, for the sake of simplicity, consider the special case in which the spacecraft slews about one axis at a time. In this case, the rate components about the other two axes go to zero. For example, for a slew about the X-axis, Eq. (5) becomes:

$$I_{SC} \begin{bmatrix} \omega_X(t) \\ 0 \\ 0 \end{bmatrix} = P(t) P^{-1}(0) TI_{RWA} \vec{\rho}(0) - TI_{RWA} \vec{\rho}(t) \equiv \vec{Q}(t) \tag{6}$$

Denote the right hand side of Eq. (6) by a new vector. $\vec{Q}(t) = [Q_X(t), Q_Y(t), Q_Z(t)]^T$. Using this notation, the first component of the vector-matrix Eq. (6) is: $I_{XX} \omega_x(t) = Q_X(t)$. In Eq. (6), both $\omega_X(t)$ and $Q_X(t)$ will take on a new value for each sample instance, t, throughout the slew, producing a new equality for each sample instance. If $\vec{\omega}_X$ and $\vec{Q}_X$ represent $N_S \times 1$ column vectors of data points from all sample instances (N_S is the total number of samples), a least-squares approach can be used to find the best estimate of I_{XX}:

$$\hat{I}_{XX} = [\vec{\omega}_X^T \vec{\omega}_X]^{-1} \vec{\omega}_X^T \vec{Q}_X \tag{7}$$

This process can be repeated for I_{YX} and I_{ZX} using the pairs of vectors $[\vec{\omega}_X, \vec{Q}_Y]$ and $[\vec{\omega}_X, \vec{Q}_Z]$, respectively. The entire process can then be repeated for slews about the Y and Z-axis as well. This process will give one estimate for each of the moments of inertia and two estimates for each one of the products of inertia (POI). The two POI estimates have been averaged together to obtain the best estimate. The results obtained are:

$$\hat{I}_{SC} = \begin{bmatrix} 8655.2 & -144 & 132.1 \\ -144 & 7922.7 & 192.1 \\ 132.1 & 192.1 & 4586.2 \end{bmatrix} \quad \text{kg-m}^2 \tag{8}$$

This estimate of the spacecraft inertia matrix is close to that determined pre-launch. Estimates for the three moments of inertia are consistently lower than their pre-launch counterparts by nearly 3%. This offset could point to a bias in the estimate of the spacecraft inertia matrix prior to launch. A bias in the pre-launch estimate is possible because the knowledge requirement for the MOI of the "dry" spacecraft is quite large: ±10%. Also, the POI estimates are within 40 kg-m^2 of their pre-launch counterparts. The magnitudes of the POI estimates are all larger than their pre-launch counterparts, which again could be evidence of a bias. Pre-launch, the knowledge requirement for the POI of the "dry" spacecraft was ±75 kg-m^2.

Instead of the "axis-by-axis" approach, the six components of the inertia tensor could also be estimated simultaneously. To this end, we first note that Eq. (6) could be written as follows:

$$\begin{bmatrix} I_{XX} & I_{XY} & I_{XZ} \\ I_{YX} & I_{YY} & I_{YZ} \\ I_{ZX} & I_{ZY} & I_{ZZ} \end{bmatrix} \begin{bmatrix} \omega_X(t) \\ \omega_Y(t) \\ \omega_Z(t) \end{bmatrix} = \begin{bmatrix} Q_X(t) \\ Q_Y(t) \\ Q_Z(t) \end{bmatrix} \tag{9}$$

The last equation, for the first time step $t = t_1$, could be re-written as:

$$\begin{bmatrix} \omega_X(t_1) & \omega_Y(t_1) & \omega_Z(t_1) & 0 & 0 & 0 \\ 0 & \omega_X(t_1) & 0 & \omega_Y(t_1) & \omega_Z(t_1) & 0 \\ 0 & 0 & \omega_X(t_1) & 0 & \omega_Y(t_1) & \omega_Z(t_1) \end{bmatrix} \begin{bmatrix} I_{XX} \\ I_{XY} \\ I_{XZ} \\ I_{YY} \\ I_{YZ} \\ I_{ZZ} \end{bmatrix} = \begin{bmatrix} Q_X(t_1) \\ Q_Y(t_1) \\ Q_Z(t_1) \end{bmatrix} \tag{10}$$

The first matrix in Eq. (10) is a 3×6 matrix. Let us denotes by S a $3N_s \times 6$ matrix consisting of a stack of 3×6 matrices for time = t_1, t_2, etc. (N_s is the total number of time steps). Let us also denotes by $\vec{\pi}$ the

6×1unknown parameter vector in Eq. (10). Finally, let us denotes by $\vec{\Gamma}$ a $3N_s \times 1$ matrix consisting of a stack of 3×1 Q vectors for time = t_1, t_2, etc.

$$S = \begin{bmatrix} \omega_X(t_1) & \omega_Y(t_1) & \omega_Z(t_1) & 0 & 0 & 0 \\ 0 & \omega_X(t_1) & 0 & \omega_Y(t_1) & \omega_Z(t_1) & 0 \\ 0 & 0 & \omega_X(t_1) & 0 & \omega_Y(t_1) & \omega_Z(t_1) \\ \vdots & \vdots & \vdots & \vdots & \vdots & \vdots \\ \omega_X(t_{Ns}) & \omega_Y(t_{Ns}) & \omega_Z(t_{Ns}) & 0 & 0 & 0 \\ 0 & \omega_X(t_{Ns}) & 0 & \omega_Y(t_{Ns}) & \omega_Z(t_{Ns}) & 0 \\ 0 & 0 & \omega_X(t_{Ns}) & 0 & \omega_Y(t_{Ns}) & \omega_Z(t_{Ns}) \end{bmatrix}, \quad \vec{\Gamma} = \begin{bmatrix} Q_X(t_1) \\ Q_Y(t_1) \\ Q_Z(t_1) \\ \vdots \\ Q_X(t_{Ns}) \\ Q_Y(t_{Ns}) \\ Q_Z(t_{Ns}) \end{bmatrix} \tag{11}$$

There is a solution to the equation $S\vec{\pi} = \vec{\Gamma}$ if the following equivalent conditions is true: (1) The column of S are linearly independent, (2) The null space of S contains only the zero vector, (3) the rank of S is $3N_s$, and (4) the square matrix S^TS is invertible. This is the case if there are in the S matrix spacecraft slew data about the X-axis, Y-axis, as well as the Z-axis. Alternatively, some of the slews should be "multi-axis" slews. In such a case, the only solution to the equation $S\vec{\pi} = \vec{\Gamma}$ is: $\vec{\pi} = [S^TS]^{-1}S^T\vec{\Gamma}$.[12]

The spacecraft mass at the start of SOI was estimated to be 4522 kg. At the end of SOI, the spacecraft mass was estimated to be about 3673.7 kg. That is, the SOI burn depleted about 848.3 kg of bi-propellant. On August 23, 2004, another long ΔV burn (Periapse Raise Maneuver, PRM) was executed, further reducing the inertia properties of the spacecraft. Accordingly, there was a significant difference between the inertia tensor before the SOI burn ($I_{Pre\text{-}SOI}$) and that after the PRM burn ($I_{Post\text{-}PRM}$). The 320-kg Probe was ejected on December 24, 2004. Again, there was a significant difference between the inertia tensor before the Probe ejection and that after the Probe ejection ($I_{Post\text{-}PROBE}$). RWA-based spacecraft slews were performed during these time periods were given in Appendix B, and data used to estimate the inertia matrix. Results are summarized in Table 1.

In Table 1, the error between the predicted and the estimated MOI values are computed using the following expression:

$$I_{Error} = (I_{Predicted} - I_{Estimated})/I_{Predicted} \times 100 \quad [\%] \tag{12}$$

For the POI, the error between the predicted and the estimated POI values are computed simply as:

$$I_{Error} = (I_{Predicted} - I_{Estimated}) \quad [kg\text{-}m^2] \tag{13}$$

Table 1. Predicted and Estimated Spacecraft Inertia Tensors in Three Different Time Windows

Parameter [kg-m^2]	Pre-SOI [Predict]	Pre-SOI [Estimate]	Pre-SOI [Error]	Post-PRM [Predict]	Post-PRM [Estimate]	Post-PRM [Error]	Post-PROBE [Predict]	Post-PROBE [Estimate]	Post-PROBE [Error]
I_{XX}	8802	8853	-0.58%	7589	7637	-0.63%	7403	7362	+0.54%
I_{YY}	8155	8171	-0.21%	6948	6948	0%	6174	6130	+0.73%
I_{ZZ}	4715	4651	+1.34%	4449	4223	+5.08%	3727	3750	-0.63%
I_{XY}	-137	-161	+24	-138	-137	-1	-129	-164	+35
I_{XZ}	+115	+114	+1	+151	+252	-102	-12	-12	0
I_{YZ}	+156	+161	-5	+150	+162	-12	+147	+149	-2

Note that the estimates for the MOI about the X and Y-axis are consistent, with errors that are less than 0.65%. Discrepancies of these sizes are acceptable because they are very small when compared with the MOI estimation accuracy requirement (±10%). The error of the MOI about the Z-axis after the Probe ejection is equally good, with error magnitude that is less than 0.65%. However, for the Pre-SOI and Post-PRM scenarios, these Z-axis MOI estimation errors are larger. These larger errors could point to one of the following possibilities: [i] A bias in the estimation process of the Z-axis MOI by the ground software, and/or [ii] The Z-axis rotation data used in the least-square estimation process are too small. In fact, with reference to Figure B2 (in Appendix B), the Z-axis rotation data are indeed very limited (relative to those associated with both X and Y-axis slews). Also, note that errors associated with the estimations of the MOI using the "combined-all-axes" approach is better than that obtained using the "axis-by-axis" approach.

The discrepancies between the POI estimates are not expressed in percents because POI could assume values that are either positive or negative. The POI estimation accuracy requirement is ±75 kg-m^2. All the POI errors given in Table 1 are smaller than the requirement except for the I_{XZ} for the post-PRM scenario.

Again, this could be due to the fact that the slew data used in the estimation of post-PRM products of inertia are too small (see, in particular, data depicted in Figure B2 in Appendix B).

V. In-Flight Calibration of the Thrusters' Magnitude[2]

Thrusters are used to perform many AACS functions. They were used to slew the spacecraft from one orientation to another during the inner Cruise phase of the mission, to detumble the spacecraft after it was separated from the launch vehicle and after the Huygens probe was ejected from the spacecraft. Thrusters are also being used to provide small trajectory corrections (also called ΔV burns). Other functions performed by the thrusters are described in Reference 2. Many of the control algorithms being used to perform these functions require knowledge of the thrusters' magnitude. The RCS ΔV control algorithm, described in greater details in the following, is one such example.

Cassini sometimes uses the four Z-facing thrusters to impart a small ΔV on the spacecraft. This is called an RCS ΔV burn. During an RCS burn, the Z-facing thrusters are used to achieve the targeted ΔV as well as to control both the X and Y-axis of the spacecraft during the burn. The X and Y-axis dead-bands of the RCS controller are both ±0.5°. At the same time, four Y-facing thrusters are used to control the spacecraft's Z-axis motion. The Z-axis dead-band of the RCS controller is ±1°. The linear momenta imparted on the spacecraft due to the firings of the four Z-facing thrusters are computed by the FSW (by multiplying the on-board FSW knowledge of the thruster magnitude by the total on-time of the four Z-facing thrusters). By dividing the computed linear momentum by the estimated mass of the spacecraft, one obtains the ΔV. The RCS ΔV burn is terminated whenever the estimated ΔV value exceeds the commanded ΔV value. This is one example where the thrusters' magnitude is used by the FSW. The ETC algorithm described in Section IV also uses the thrusters' magnitude.

The monopropellant propulsion system for Cassini is of the blow-down type. With this system, the hydrazine tank pressure, which was about 2635 kPa at Launch, will decay slowly with time as hydrazine is depleted through thruster firings. At launch (October 15, 1997), the thrust magnitude was about 0.97 N. By the time of Saturn Orbit Insertion (June 30, 2004), the thrust magnitude had decayed to 0.75 N. During Probe relay tracking (January 14, 2005), the thrust magnitude was 0.69 N. The monopropellant tank will be "recharged" only once, which is currently planned in April 2006.

The Propulsion team estimates the time-varying magnitudes of eight A-branch and another eight B-branch thrusters. Magnitudes of the eight thrusters on the A-branch are represented by one mean value in the AACS flight software, those for the B-branch thrusters are represented by another value. These thruster magnitudes are updated from time to time to reflect the decaying thrust.

Cassini RCS thrusters were characterized during flight acceptance testing. One set of test results is captured by an equation that relates the nominal steady state RCS thrust to the pressure of the hydrazine tank. Thruster magnitude estimated via this equation has been further verified in flight by the Propulsion team.[10] Such an in-flight confirmation is necessary because accurate calibrations of the thrusters prior to flight were limited by various factors. Among these is the difficulty of maintaining a suitable vacuum in a chamber during thruster calibration, while gas is discharged from the thruster. Commonly, it is difficult to predict and establish, during ground testing, the exact temperature and pressure conditions under which the thrusters will operate in-flight. The output direction of the thrust will not necessarily be concentric with the expansion nozzle. The uncertainty associated with this thrust equation is on the order of ±5-10%.

There is an AACS-centric approach that could also be used to independently determine the RCS thrusters' magnitudes. The underlying principle of the AACS approach is the Euler's equation. In-flight, in two sets of special events (RWA drag torque run-down test and RWA biasing), the reaction wheels are powered on while eight thrusters maintain the spacecraft's attitude. Changes in the reaction wheels' rates (during RWA biasing or drag torque run-down test) produce reaction torque on the spacecraft and hence thruster firings. RWA spin rate data collected from these events could be used to calibrate the thrusters. Details associated with the RWA biasing event are given below to illustrate the underlying principle. The general principle is identical to that described in references 9 and 11. The effectiveness of the approach is demonstrated by its applications on several sets of flight data, also given below.

A representative reaction wheel biasing is carried out as follows, the spacecraft is Earth-pointed and is on thruster control, with dead-bands of [2, 2, 2] mrad. After being powered on, the reaction wheels are spun up to attain a set of pre-selected spin rates. In so doing, the D.C. motors of the RWAs impart equal and opposite torque on the spacecraft. Thrusters are then fired to maintain the spacecraft's attitude in the

presence of these reaction torques. The rotational motion of the spacecraft during a RWA biasing event is governed by Euler equation:

$$I_{SC}\dot{\vec{\omega}} + \vec{\omega} \times (I_{SC}\vec{\omega} + \vec{H}_{RWA}) + \dot{\vec{H}}_{RWA} = \vec{T}_{PMS} \tag{14}$$

In Eq. (14), I_{SC} is the S/C's inertia tensor. The spacecraft rate vector, ω, is estimated by the attitude estimator. The total angular momentum vector of the three reaction wheels, in the spacecraft mechanical frame, H_{RWA}, is available from the RWA "manager." Torque vector exerted on the spacecraft due to thruster firing, T_{PMS}, is available from the propulsion "manager." Taking the time integration of the Equation (14), from time = 0 to time = t_i, we have:

$$I_{SC}\{\vec{\omega}(t_i) - \vec{\omega}(0)\} + \{\vec{H}_{RWA}(t_i) - \vec{H}_{RWA}(0)\} + \int_0^{t_i} \vec{\omega} \times (I_{SC}\vec{\omega} + \vec{H}_{RWA})dt \approx \int_0^{t_i} \vec{T}_{PMS}dt \tag{15}$$

This is an approximate equation because the small angular momentum accumulated due to the non-gravitational torque has been neglected. Let us simplify this equation using the following notations. Let $\Delta\omega(t_i) = \omega(t_i) - \omega(0)$, $\Delta H_{RWA}(t_i) = H_{RWA}(t_i) - H_{RWA}(0)$, $\Delta G(t_i) = \int \omega \times (I_{SC}\omega + H_{RWA})\, dt$, where the integration is from t = 0 to t_i. The per-axis angular impulses imparted on the spacecraft due to thruster firings are determined as follows. The coordinates of the locations of the eight A-branch thrusters, Z_1, Z_2, Z_3, Z_4, Y_1, Y_2, Y_3, and Y_4 are given by: $[+L_X, +L_Y, +L_{ZZ}]$, $[-L_X, +L_Y, +L_{ZZ}]$, $[-L_X, -L_Y, +L_{ZZ}]$, $[+L_X, -L_Y, +L_{ZZ}]$, $[+L_X, +L_Y, +L_{ZY}]$, $[-L_X, +L_Y, +L_{ZY}]$, $[-L_X, -L_Y, +L_{ZY}]$, and $[+L_X, -L_Y, +L_{ZY}]$. Here, L_X = 1.234 m, L_Y = 1.580 m, L_{ZY} = 2.880 m, and L_{ZZ} = 3.019 m. Let $[e_X, e_Y, e_Z]$ denotes the coordinates of the S/C's center of mass, and Q (3×8) denotes the moment matrix from the eight thrusters Z_1, Z_2, Z_3, Z_4, Y_1, Y_2, Y_3, and Y_4 (with magnitudes of F_1, F_2, F_3, F_4, F_5, F_6, F_7, and F_8, respectively) to the three S/C's coordinate axes:

$$Q = \begin{bmatrix} -(L_Y - e_Y) & -(L_Y - e_Y) & +(L_Y + e_Y) & +(L_Y + e_Y) & +(L_{ZY} - e_Z) & +(L_{ZY} - e_Z) & -(L_{ZY} - e_Z) & -(L_{ZY} - e_Z) \\ +(L_X - e_X) & -(L_X + e_X) & -(L_X + e_X) & +(L_X - e_X) & 0 & 0 & 0 & 0 \\ 0 & 0 & 0 & 0 & -(L_X - e_X) & +L_X + e_X & -L_X - e_X & +L_X - e_X \end{bmatrix} \tag{16}$$

Using these notations, we have $\int T_{PMS}\, dt = Q \bullet [F_1\Delta\tau_1(t_i), \ldots, F_8\Delta\tau_8(t_i)]^T$, where $\Delta\tau_1(t_i)$ denotes the Z_1 thruster's incremental on-time from t = 0 to t = t_i, and $\Delta\tau_8(t_i)$ denotes the Y_4 thruster's incremental on-time from t = 0 to t = t_i. Equation (15) is now denoted compactly by the following expression:

$$I_{SC}\Delta\omega(t_i) + \Delta H_{RWA}(t_i) + \Delta G(t_i) = Q \bullet [F_1\Delta\tau_1(t_i), \ldots, F_8\Delta\tau_8(t_i)]^T \tag{17}$$

If we assume that the Z-facing thrusters are mounted <u>exactly</u> parallel to the S/C's Z-axis, and the Y-facing thrusters are mounted <u>exactly</u> parallel to the Y-axis, then equation (17) could be decoupled into two "components." This is because the Z-facing thrusters' firings only impart torque about the S/C's X and Y-axis, and Y-facing thrusters' firings (in pair) only impart torque about the S/C's Z-axis. The [X, Y] rows of equation (17), for time $t_i = t_1$, could be denoted by:

$$\begin{bmatrix} \{I_{SC}\Delta\omega(t_1) + \Delta H_{RWA}(t_1) + \Delta G(t_1)\}_X \\ \{I_{SC}\Delta\omega(t_1) + \Delta H_{RWA}(t_1) + \Delta G(t_1)\}_Y \end{bmatrix} = \begin{bmatrix} Q_{11}\Delta\tau_1(t_1) & Q_{12}\Delta\tau_2(t_1) & Q_{13}\Delta\tau_3(t_1) & Q_{14}\Delta\tau_4(t_1) \\ Q_{21}\Delta\tau_1(t_1) & Q_{22}\Delta\tau_2(t_1) & Q_{23}\Delta\tau_3(t_1) & Q_{24}\Delta\tau_4(t_1) \end{bmatrix} P_Z \tag{18}$$

Here, $P_Z = [F_1, F_2, F_3, F_4]^T$, is the unknown Z-facing thruster magnitude vector. Equations similar to (18) could be written for time steps $t_2, \ldots, t_N$ where N is the total number of time steps. All these equations could be stacked together to form the following "composite" matrices:

$$V_{XY} = \begin{bmatrix} \{I_{SC}\Delta\omega(t_1) + \Delta H_{RWA}(t_1) + \Delta G(t_1)\}_X \\ \{I_{SC}\Delta\omega(t_1) + \Delta H_{RWA}(t_1) + \Delta G(t_1)\}_Y \\ \vdots \\ \{I_{SC}\Delta\omega(t_N) + \Delta H_{RWA}(t_N) + \Delta G(t_N)\}_X \\ \{I_{SC}\Delta\omega(t_N) + \Delta H_{RWA}(t_N) + \Delta G(t_N)\}_Y \end{bmatrix}, \quad U_{XY} = \begin{bmatrix} Q_{11}\Delta\tau_1(t_1) & Q_{12}\Delta\tau_2(t_1) & Q_{13}\Delta\tau_3(t_1) & Q_{14}\Delta\tau_4(t_1) \\ Q_{21}\Delta\tau_1(t_1) & Q_{22}\Delta\tau_2(t_1) & Q_{23}\Delta\tau_3(t_1) & Q_{24}\Delta\tau_4(t_1) \\ \vdots & & & \\ Q_{11}\Delta\tau_1(t_N) & Q_{12}\Delta\tau_2(t_N) & Q_{13}\Delta\tau_3(t_N) & Q_{14}\Delta\tau_4(t_N) \\ Q_{21}\Delta\tau_1(t_N) & Q_{22}\Delta\tau_2(t_N) & Q_{23}\Delta\tau_3(t_N) & Q_{24}\Delta\tau_4(t_N) \end{bmatrix} \tag{19}$$

Note that V_{XY} is a 2N × 1 matrix and U_{XY} is a 2N × 4 matrix. The least-square solution of P_Z is then given by $P_Z = \{U^T_{XY}U_{XY}\}^{-1}U^T_{XY}V_{XY}$.

Similarly, the Z-axis row of equation (17), for time $t = t_1,\ldots,t_N$, could be denoted by $U_Z \bullet P_Y = V_Z$. Here, $P_Y = [F_5, F_6, F_7, F_8]^T$, is the unknown Y-facing thruster magnitude vector, V_Z is a N×1 matrix, and U_Z is a N×4 matrix:

$$V_Z = \begin{bmatrix} \{I_{SC}\Delta\omega(t_1)+\Delta H_{RWA}(t_1)+\Delta G(t_1)\}_Z \\ \vdots \\ \{I_{SC}\Delta\omega(t_N)+\Delta H_{RWA}(t_N)+\Delta G(t_N)\}_Z \end{bmatrix}, \quad U_Z = \begin{bmatrix} Q_{35}\Delta\tau_5(t_1) & Q_{36}\Delta\tau_6(t_1) & Q_{37}\Delta\tau_7(t_1) & Q_{38}\Delta\tau_8(t_1) \\ \vdots & \vdots & \vdots & \vdots \\ Q_{35}\Delta\tau_5(t_N) & Q_{36}\Delta\tau_6(t_N) & Q_{37}\Delta\tau_7(t_N) & Q_{38}\Delta\tau_8(t_N) \end{bmatrix} \tag{20}$$

However, the determination of P_Y using equation (20) will encounter the following difficulty. With reference to the third row of equation (16), since e_X is typically very small compared to L_X, the (3,5) element of *Q* is almost equal to the (3,7) element. Similarly, the (3,6) and (3,8) elements of *Q* are almost identical. As such, one might not be able to estimate the *individual* magnitudes of the four Y-facing thrusters via the least-square fit: $P_Y = \{U^T_Z U_Z\}^{-1} U^T_Z V_Z$. This is the case because {Y_1 and Y_3} and {Y_2 and Y_4} are always fired in pairs. Hence, the rank of the matrix U_Z is 2 instead of 4. To overcome this difficulty, let us define the following new vector and matrix: P_{YY} (2×1) = $[(F_5 + F_7)/2, (F_6 + F_8)/2]^T$, and U_{ZZ} is an N × 2 matrix:

$$U_{ZZ} = \begin{bmatrix} Q_{35}\Delta\tau_5(t_1)+Q_{37}\Delta\tau_7(t_1) & Q_{36}\Delta\tau_6(t_1)+Q_{38}\Delta\tau_8(t_1) \\ \vdots & \vdots \\ Q_{35}\Delta\tau_5(t_N)+Q_{37}\Delta\tau_7(t_N) & Q_{36}\Delta\tau_6(t_N)+Q_{38}\Delta\tau_8(t_N) \end{bmatrix} \tag{21}$$

The least square fit result is: $P_{ZZ} = \{U^T_{ZZ} U_{ZZ}\}^{-1} U^T_{ZZ} V_Z$. The estimated magnitudes of the Y-facing thrusters are: $F_5 = F_7 = P_{ZZ}(1,1)$, and $F_6 = F_8 = P_{ZZ}(2,1)$. Finally, we might want to just estimate the mean value of the four Y-facing thrusters. Again, let us define the following new vector and matrix: P_{YYY} (1×1) = $(F_5 + F_6 + F_7 + F_8)/4$, and U_{ZZZ} is an N × 1 matrix:

$$U_{ZZZ} = \begin{bmatrix} Q_{35}\Delta\tau_5(t_1)+Q_{36}\Delta\tau_6(t_1)+Q_{37}\Delta\tau_7(t_1)+Q_{38}\Delta\tau_8(t_1) \\ \vdots \\ Q_{35}\Delta\tau_5(t_N)+Q_{36}\Delta\tau_6(t_N)+Q_{37}\Delta\tau_7(t_N)+Q_{38}\Delta\tau_8(t_N) \end{bmatrix} \tag{22}$$

The least square fit result is: $P_{ZZZ} = \{U^T_{ZZZ} U_{ZZZ}\}^{-1} U^T_{ZZZ} V_Z$. The magnitudes of the Y-facing thrusters are: $F_5 = F_6 = F_7 = F_8 = P_{ZZZ}(1,1)$.

In flight, the AACS and PMS teams typically generate only *one* thruster magnitude estimate for the eight A-branch thrusters and another *one* estimate for the eight B-branch thrusters. This single estimate could be estimated using the following matrices: V_{XYZ} (3N×1) and U_{XYZ} (3N×1). The mean magnitude of the eight thrusters are then given by: $F_1 = F_2 = F_3 = F_4 = F_5 = F_6 = F_7 = F_8 = \{U^T_{XYZ} U_{XYZ}\}^{-1} U^T_{XYZ} V_{XYZ}$.

$$V_{XYZ} = \begin{bmatrix} \{I_{SC}\Delta\omega(t_1)+\Delta H_{RWA}(t_1)+\Delta G(t_1)\}_X \\ \{I_{SC}\Delta\omega(t_1)+\Delta H_{RWA}(t_1)+\Delta G(t_1)\}_Y \\ \{I_{SC}\Delta\omega(t_1)+\Delta H_{RWA}(t_1)+\Delta G(t_1)\}_Z \\ \vdots \\ \{I_{SC}\Delta\omega(t_N)+\Delta H_{RWA}(t_N)+\Delta G(t_N)\}_X \\ \{I_{SC}\Delta\omega(t_N)+\Delta H_{RWA}(t_N)+\Delta G(t_N)\}_Y \\ \{I_{SC}\Delta\omega(t_N)+\Delta H_{RWA}(t_N)+\Delta G(t_N)\}_Z \end{bmatrix},$$

$$U_{XYZ} = \begin{bmatrix} Q_{11}\Delta\tau_1(t_1)+Q_{12}\Delta\tau_2(t_1)+Q_{13}\Delta\tau_3(t_1)+Q_{14}\Delta\tau_4(t_1)+Q_{15}\Delta\tau_5(t_1)+Q_{16}\Delta\tau_6(t_1)+Q_{17}\Delta\tau_7(t_1)+Q_{18}\Delta\tau_8(t_1) \\ Q_{21}\Delta\tau_1(t_1)+Q_{22}\Delta\tau_2(t_1)+Q_{23}\Delta\tau_3(t_1)+Q_{24}\Delta\tau_4(t_1) \\ Q_{35}\Delta\tau_5(t_1)+Q_{36}\Delta\tau_6(t_1)+Q_{37}\Delta\tau_7(t_1)+Q_{38}\Delta\tau_8(t_1) \\ \vdots \\ Q_{11}\Delta\tau_1(t_N)+Q_{12}\Delta\tau_2(t_N)+Q_{13}\Delta\tau_3(t_N)+Q_{14}\Delta\tau_4(t_N)+Q_{15}\Delta\tau_5(t_N)+Q_{16}\Delta\tau_6(t_N)+Q_{17}\Delta\tau_7(t_N)+Q_{18}\Delta\tau_8(t_N) \\ Q_{21}\Delta\tau_1(t_N)+Q_{22}\Delta\tau_2(t_N)+Q_{23}\Delta\tau_3(t_N)+Q_{24}\Delta\tau_4(t_N) \\ Q_{35}\Delta\tau_5(t_N)+Q_{36}\Delta\tau_6(t_N)+Q_{37}\Delta\tau_7(t_N)+Q_{38}\Delta\tau_8(t_N) \end{bmatrix} \tag{23}$$

Before applying the technique described above on flight data, we first applied it on data generated using a simulation test bed. The test environment used was the Flight Software Development System (FSDS).[13] FSDS is an all software closed-loop, workstation-based, faster than real-time test bed. It was the

primary testing environment used by Cassini attitude control flight software engineers to develop and validate AACS flight software. Key features of FSDS are the high-fidelity modeling of attitude control actuators, sensors, spacecraft dynamics (including structural flexibilities and those due to fuel sloshing), AACS bus models, fault injection, star simulation, and many other features. Unlike the flight data, FSDS-based simulation data of the spacecraft's per-axis rate, reaction wheel rates, thrusters' on-times are generated at regular intervals of once per second. Moreover, the "unknown" thruster magnitude to be estimated is a known value specified by the tester in the generation of the simulation data. As such, it is convenient to use FSDS data to flush out any incorrect assumptions made in the derivation of the least-square technique described by equation (23).

For simplicity, all the eight thrusters were assumed the same thruster magnitude of 0.75 N. The spacecraft's moments of inertia and products of inertia used in the simulation were: I_{XX} = 7375.02 kg-m^2, I_{YY} = 6061.58 kg-m^2, I_{ZZ} = 3829.70 kg-m^2, I_{XY} = -136.58 kg-m^2, I_{XZ} = +6.23 kg-m^2, and I_{YZ} = 180.26 kg-m^2. These inertia properties were estimated using the approach that is described in Section IV. Inertia properties of the three reaction wheels are: I_{RWA1} = 0.161 kg-m^2, I_{RWA2} = 0.160 kg-m^2, and I_{RWA3} = 0.161 kg-m^2. The test scenario selected involves the biasing of the three reaction wheels from an identical initial spin rate of zero rpm to an identical final spin rate of 1800 rpm. The torque generated by the reaction wheels' D.C. motors to effect these rate changes will produce a reaction torque vector that is aligned with the minus Z-axis of the spacecraft. As such, only the Y2 and Y4 thrusters are fired to negate the reaction torque. Time histories of the reaction wheels' spin rates and the on-times of both the Y2 and Y4 thrusters are given in Appendix C. The computed value of the thrusters' magnitude is 0.98 N, about 30% *higher* than the "truth" value of 0.75 N.

A likely source of error is an incorrect assumption made in the estimation of angular impulses imparted on the spacecraft due to thrusters' firings. Equation (17) was derived assuming $\int T_{PMS}\, dt = Q \bullet [F_1 \Delta\tau_1(t_i), \ldots, F_8 \Delta\tau_8(t_i)]^T$. To arrive at this expression, we had (incorrectly) assumed that the thrusters respond "instantaneously" to their firing commands. In reality, there is a "on/off" delay time (τ_{Delay}) between the firing command and the time thrust begins to appear. The main sources of the delay include the delay time of the valve open/close electronics as well as the time it takes the propellant to flow from the valve to the injector. Thereafter, the thrust increases with time exponentially with a time constant (τ_{Rise}) to its steady state value of F ($F = F_1 = F_2 = \cdots = F_8$). After the termination of the firing command, the thrust will stay at its current value for another τ_{Delay} second. It then decays to zero exponentially with a time constant of τ_{Fall}. These rise and fall times are due mainly to the inertia of the fuel (hydrazine), and the inertia of chemical decompositions of the hydrazine (N_2H_4) when it was injected into the catalyst bed. The decomposition of hydrazine leads first to hydrogen and ammonia. The ammonia further decomposes into hydrogen and nitrogen.[14]

$$\begin{aligned} 3N_2H_4 &\rightarrow 4NH_3 + N_2 \\ 4NH_3 &\rightarrow 2N_2 + 6H_2 \end{aligned} \tag{24}$$

The rates of these chemical reactions are functions of the temperature of the catalyst bed; time constants are smaller with "hot" thrusters and larger with "cold" thrusters.

The values of τ_{Delay}, τ_{Rise}, and τ_{Fall}, as estimated by the thruster manufacturer, are 5, 20, and 65 ms (milli-second = 10^{-3} s), respectively. These values come from extensive thruster testing with feed pressures of 100, 240 and 400 psia. For the Cassini monopropellant system, the feed pressure was about 255 psia in 2005 but it will increase to 400 psia after a planned recharge of the monopropellant tank assembly in April 2006. Test results indicated that the rise time constant varied from 15 to 25 ms (with a mean value of about 20 ms). Test results also indicated that the fall time constant varied from 40 to 90 ms (with a mean time constant of 65 ms). These thruster force characteristics are all implemented in the thruster model of FSDS.

It is obvious that for as long as $\tau_{Fall} > \tau_{Rise}$, the effective impulse is larger than 0.75×0.125 Ns, which is what was assumed in Equation (17). It can be shown that for a commanded "on time" of Δs, the actual impulse (area under the curve; thrust-time history) is $F\times(\Delta+\tau_{Fall})+F\times\tau_{Rise}\times\{\exp[-\Delta/\tau_{Rise}]-\exp[-\tau_{Delay}/\tau_{Rise}]\}-F\times(\tau_{Fall}+\tau_{Delay})\times\exp[-\Delta/\tau_{Rise}]$. The ratio of the actual impulse and the impulse assumed by Equation (17) could then be computed. For a 125-ms on-time command, the ratio is 1.395. For a 250-ms on-time command, the ratio is 1.198. In the RWA biasing scenario considered, the total firing time of the Y2 thruster (which is identical to that of the Y4 thruster) is 21.875 seconds. This firing time comprises of 133 125-ms pulses, 16 250-ms pulses, one 500-ms pulse, and one 750-ms pulse. For the rise and fall time constants specified above, the ratio of the actual and the "ideal" impulse for this particular scenario is

1.3406. If this ratio is taken into account, the estimated thrust level is 0.98/1.3406≈0.731 N. This estimated thrust magnitude is closer to the 0.75-N thrust magnitude assumed in the FSDS simulation value.

Next, we apply the same methodology to five sets of flight data associated with five RWA biasing events that were performed after the Probe ejection event. First apply the inertia tensor calibration technique (see Section IV) on a set of per-axis slew data. These are slews that were performed for the purpose of a gyroscope calibration. The values of the calibrated inertia properties are listed in Table 1 (labeled "Post Probe"). Without taking into account the effect due to thrusters' dynamics, the calibrated thrusters' magnitudes are given in the 4th column of Table 2.

Table 2. Predicted and Estimated Thrusters' Magnitudes in Five RWA Biasing Events

Days in 2004 of RWA Biasing	Biased Rates of RWA-1, RWA-2, & RWA-3 [rpm]			Predicted Thruster Magnitude [N]	Estimated Thruster Magnitude (No Adjustment) [N]	Estimated Thruster Magnitude (τ_{Decay} = 65 ms) [N]	Estimated Thruster Magnitude (τ_{Decay} = 40 ms) [N]
28	-794	-870	-296	0.699	0.80	0.573	0.669
49	1026	922	836		0.79	0.566	0.661
61	246	-473	-928		0.82	0.588	0.686
71	-1004	226	-407		0.81	0.581	0.678
94	-949	-672	-674		0.83	0.595	0.695

Comparisons of the actual and the calibrated thrusters' magnitudes made with FSDS data indicate the need to adjust for the effects of the thrusters' dynamics. The thrusters' magnitudes estimated without taking into account thrusters' dynamics must be divided by R to produce the final thrusters' magnitude estimate. For the RWA biasing performed on day 28 of 2004, the total on-times of the eight thrusters are 0.74, 1.72, 4.28, 3.31, 9.81, 0.375, 9.81, and 0.375 s for thruster Z_1, …,Y_4, respectively. The mean sizes of the thruster pulses are: 123, 115, 122, 127, 131, 94, 131, and 94 ms for thruster Z_1,…,Y_4, respectively. The sizes of most of the thrusters' pulses are 125 ms (other than those associated with the Y_2 and Y_4 thrusters. But the total on-time of each of these two Y-facing thruster is only 1.23% of the total on-time of all the thrusters). For 125-msec thrusters' pulses, R =1.395 if τ_{Rise} = 20 ms and τ_{Decay} = 65 ms. If the actual value of τ_{Decay} is 40 ms, then R =1.195 (with τ_{Rise} = 20 ms). In Table 2, we note that the thrusters' magnitudes estimated with a decay time constant of 40 ms are very close to their "predicted" values. The uncertainty associated with the actual values of τ_{Rise} and τ_{Decay} makes it difficult to estimate the thrusters' thrust level with good accuracy. The error of the estimated thruster's magnitude is on the order of ±10%.

VI. Summary and Conclusions

The Cassini Attitude and Articulation Control Subsystem is the subsystem that must satisfy the most science and mission requirements, to meet these challenging requirements, knowledge of the spacecraft's inertia matrix as well as thrusters' magnitude, among other spacecraft parameters, are needed. In this paper, we describe two similar methodologies that were used by the Cassini attitude control team to determine these key parameters. The methodology used to estimate the inertia tensor takes advantage of the fact that the totalThe angular momentum vector of a spacecraft, as expressed in an inertial coordinate system, is conserved during reaction wheel slews. The methodology used to estimate thruster magnitude relates changes in the total angular momentum vector of the spacecraft with that generated by the firings of thrusters. The spacecraft's inertia matrix estimated using the proposed "conservation of angular momentum" methodology agreed very well with those predicted on the ground. The estimated accuracy of the proposed methodology is on the order of ±1%. Thrusters' magnitude estimated using the proposed methodology is in general agreement with those predicted by a propulsion model. However, the accuracy of the proposed approach is affected by the time-varying nature of thrust level when thrusters are operated in "pulse" mode. Additionally, telemetry data of thrusters' on-time are typically available only once every tenth of seconds. As such, the estimated accuracy of the proposed methodology is poor and only on the order of ±10%.

Acknowledgements

The work described in this paper was carried out by Jet Propulsion Laboratory, California Institute of Technology, under a contract with the National Aeronautics and Space Administration. The authors wish to thank Mr. Jay Brown, Cassini AACS Flight Software Lead Engineer, for many helpful discussions on the Flight Software Development System, FSDS and Mr. William Breckenridge, a senior member of the Guidance, Navigation, and Control Section, who improved the technical accuracy of this paper through his careful reading. Any remaining errors of fact or interpretation are of course our responsibility.

References

[1]Jaffe, L. and Herrell, L., "Cassini Huygens Science Instruments, Spacecraft, and Mission," *Journal of Spacecraft and Rockets*, Vol. 34, No. 4, 1997, pp. 509-521.

[2]Lee, A.Y. and Hanover, G., "Cassini Spacecraft Attitude Control System Flight Performance," *Proceedings of the AIAA Guidance, Navigation, and Control Conference*, San Francisco, California, August 15-18, 2005.

[3]Wong, E. and Breckenridge, W., "An Attitude Control Design for the Cassini Spacecraft," *Proceedings of the AIAA Guidance, Navigation, and Control Conference*, AIAA, Washington, D.C., 1995, pp. 931-945.

[4]Macala, G.A., "Design of the Reaction Wheel Attitude Control System for the Cassini Spacecraft," Paper AAS 02-121, AAS/AIAA Space Flight Mechanics Meeting, San Antonio, Texas, January 27-30, 2002.

[5]Lee, A.Y. and Wertz, J., "In-Flight Calibration of the Cassini Spacecraft Inertia Matrix," *Journal of Spacecraft and Rockets*, Vol. 39, No. 1, January-February, 2002, pp. 153-155.

[6]Wertz, J. and Lee, A.Y., "Inflight Estimation of the Cassini Spacecraft's Inertia Tensor," *Proceedings of the 11th AAS/AIAA Space Flight Mechanics Meeting*, Santa Barbara, California, Feb. 11-15, 2001.

[7]Lee, A.Y., "Model-based Thruster Leakage Monitor for the Cassini Spacecraft," *Journal of Spacecraft and Rockets*, Vol. 36, No. 5, September-October, 1999, pp. 745-749.

[8]Enright, P., "Thrust Vector Control Algorithm Design for the Cassini Spacecraft," Paper AIAA 93-1043, *Proceedings of the AIAA/AHS/ASEE Aerospace Design Conference*, Irvine, California, February 1993.

[9]Wu, S.F., Steyn, W.H., and Bordany, R.E., "In-orbit Thruster Calibration Techniques and Experiment Results with UoSAT-12," *Control Engineering Practice*, 12 (2004), pp. 87-98.

[10]Barber, T.J. and Cowley, R.T., "Initial Cassini Propulsion System In-Flight Characterization," AIAA-2002-4152. 38th AIAA/ASME/SAE/ASEE Joint Propulsion Conference and Exhibit, Indianapolis, Indiana, July 7-10, 2002.

[11]Wiktor, P.J., "On-orbit Thruster Calibration," *Journal of Guidance, Control, and Dynamics*, Vol. 19, No. 4, 1996, pp. 934-940.

[12]Strang, G., "Linear Algebra and Its Applications," *Academic Press, Inc.*, 2nd edition, 1980.

[13]Brown, J., Lam, D., Chang, L., Burk, T., and Wette, M., "The Role of Flight Software Development System Simulator throughout the Cassini Mission," Proceedings of the 2005 AIAA Guidance, Navigation, and Control Conference, San Francisco, California, August 15-18, 2005.

[14]Koelle, H.H. (editor), "Handbook of Astronautical Engineering," 1st edition, 1961.

Appendix A
Non-Gravitational Torque Imparted on the Spacecraft During Cruise and Tour

The Probe was ejected on December 24, 2004 (9.055 A.U.). After the ejection, the spacecraft was detumbled and slewed back to an Earth-pointed attitude by thrusters. Thereafter, a thruster-to-reaction wheel control mode transition was made and the spacecraft was maintained in that Earth-pointed attitude by the reaction wheels. Non-gravitational torque that is significant during this time includes only the body-fixed RTG torque and the direct solar radiation torque. The presence of this non-gravitational torque on the spacecraft caused the spin rates of the reaction wheels to "drift" slowly with time. Let the vector $\Delta\omega_{RWA}$, in rpm, be the change in the spin rates of the three reaction wheels over a period of time T_{Earth} (in s). Since the

spacecraft was quiescent throughout this time period, the non-gravitational torque T_{nongra} can be estimated by:

$$\vec{T}_{nongra} \approx \begin{bmatrix} 0 & -\frac{1}{\sqrt{2}} & +\frac{1}{\sqrt{2}} \\ \sqrt{\frac{2}{3}} & -\frac{1}{\sqrt{6}} & -\frac{1}{\sqrt{6}} \\ +\frac{1}{\sqrt{3}} & +\frac{1}{\sqrt{3}} & +\frac{1}{\sqrt{3}} \end{bmatrix} \left(\frac{\Delta\vec{\omega}_{RWA} \times 2\pi}{60}\right) \times \frac{0.16}{T_{Earth}} \quad \text{Nm}$$

In this expression, we have used a mean moment of inertia of 0.16 kg-m^2 for each RWA. The coordinate transformation matrix, from the RWA to the spacecraft mechanical frame, is given in Figure 4. Estimated total non-gravitational torques imparted on the spacecraft, without the Probe, in an HGA-to-Earth attitude, and at about 9.055 A.U., are given in Table A1.

Table A1. Estimated Non-gravitational Torque During Tour With an Earth-Pointed Attitude (9.055 A.U.)

	X-axis Torque (μNm)	Y-axis Torque (μNm)	Z-axis Torque (μNm)
Total	-0.53	-2.11	+1.83
RTG	-2.36	-2.21	+1.83
Solar	+1.83	+0.1	0

Appendix B
Spacecraft Slew Data Used in the Estimations of Inertia Tensor

The time histories of the per-axis S/C rates for the "Pre-SOI", "Post-PRM", and "Post-PROBE" scenarios are given in Figures B1, B2, and B3, respectively. In these figures, the horizontal axes are time in units of second. The vertical axes are S/C per-axis rates in units of mrad/s.

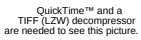

Figure B1. Time Histories of S/C Rates Used in Calibration of Inertia Tensor (Pre-SOI, 03-DOY-058)

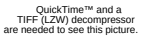

Figure B2. Time Histories of S/C Rates Used in Calibration of Inertia Tensor (Post-PRM, 04-DOY-279)

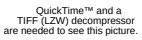

Figure B3. Time Histories of S/C Rates Used in Calibration of Inertia Tensor (Post-PROBE, 05-DOY-040)

Appendix C

Reaction Wheels' Spin Rates and Thrusters' On-time Used in the Estimations of Thruster Magnitude

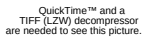

Figure C1. Time histories of Reaction Wheels' Spin Rates

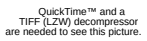

Figure C2. Time Histories of Y2 and Y4 Thrusters' On-times

Appendix D

Use of Accelerometer Data to Calibrate the Z-facing Thrusters' Magnitude[2]

There is yet another way to estimate the mean magnitude of the four Z-facing thrusters. This method uses the thrusters' *on-time* data collected from a thruster-based ΔV burn as well as the ΔV estimate made using an accelerometer. The accelerometer is typically not powered on during a thruster-based ΔV burn. But, for the purpose of this calibration, we will power it on. It will provide accurate estimate of the ΔV imparted on the spacecraft due to the firing of the Z-facing thrusters. Let ΔT_{zi} ,in seconds, be the "on-time" of thruster Z_i (i=1-4) for a particular RCS ΔV burn, ΔV (in m/s) be the magnitude of the spacecraft's velocity change as estimated by the accelerometer, and M_{SC} is the spacecraft mass. The ΔV magnitude detected by the accelerometer is given by:

ΔV (in m/s) = $\Delta V_{dn} \times 2.0202\text{e-}3$ m/s/dn + $Bias_{ACC} \times T_{Burn}$

Here, ΔV_{dn} (in dn) is the number of data number reported by the accelerometer ,ACC, across the ΔV burn, the scale factor of the accelerometer (as determined on the ground) is 2.0202 mm/s per data number, the bias of the accelerometer, $bias_{ACC}$, in m/s^2, could be easily determined by the time rate of change of the accelerometer's output data after it has been powered on (but before the start of the burn), and T_{Burn} ,in s, is the duration of the RCS ΔV burn. Invoking the conservation of the linear momentum along the Z-axis of the spacecraft, the mean magnitude of the four Z-facing thruster could be estimated via:

$F_1 = F_2 = F_3 = F_4 = M_{SC} \times \Delta V / (\Delta\tau_{Z1} + \Delta\tau_{Z2} + \Delta\tau_{Z3} + \Delta\tau_{Z4})$.

The last equation was written assuming that both the Z-facing thrusters and the accelerometer are mounted parallel to the spacecraft's Z-axis. The misalignment of the accelerometer's sensing axis relative to the Z-axis is bounded by about 0.1°. That of the Z-facing thrusters' thrust is on the order of 1°. Since $\cos(0.1°) \approx \cos(1°) \approx 1$, the errors introduced by the misalignments in the last equation are quite small.